



Cite this: DOI: 10.1039/d0tc05243d

Sulfonatocalix[4]arene-based light-harvesting amphiphilic supramolecular assemblies for sensing sulfites in cells†‡

Zhixue Liu, Xiaohan Sun, Xianyin Dai, Jingjing Li, Peiyu Li and Yu Liu *

Herein, we reported highly efficient light-harvesting amphiphilic supramolecular assemblies based on a tetraphenylethylene derivative (TPE-4Py), an amphiphilic sulfonatocalix[4]arene (SC4A-C6), and a sulfite fluorescent probe (SP). The obtained assemblies not only showed obvious signal amplification compared to SP alone, with an antenna effect of up to 28.1 based on highly efficient energy transfer of 75.2% from TPE-4Py/SC4A-C6 to SP, but also displayed an excellent ratiometric fluorescence signal output toward sulfites. Meanwhile, the assemblies showed no obvious cytotoxicity to A549 cells and could be used to sense sulfites in the cells. This strategy for constructing supramolecular assemblies not only resulted in a high-efficiency light-harvesting platform but also amplified the signal of the probe because of the high antenna effect and thus constitutes an effective method for fabricating fluorescent cell sensors.

Received 7th November 2020,
Accepted 23rd December 2020

DOI: 10.1039/d0tc05243d

rsc.li/materials-c

Introduction

Light-harvesting systems (LHSs) that exhibit a high antenna effect have found widespread application in various fields, including biological imaging and optoelectronics.¹ Multichromophoric macromolecules have potential utility for this purpose. For example, in 1996, Lehn and co-workers reported that a merocyanine dye and a β -cyclodextrin bearing seven naphthoyl chromophores form stable 1:1 complexes that show 100% energy-transfer efficiency.² The behavior of such multichromophoric cyclodextrins mimics the antenna effect observed in photosynthesis, and they show great promise as photochemical microreactors. After that, a diverse array of other materials have been employed to fabricate LHSs, including organic nanocrystals,³ metal complexes,⁴ metallacycles,⁵ surface-cross-linked micelles,^{6,7} peptide-modulated chromophores,⁸ DNA oligonucleotides,⁹ organic-inorganic hybrid materials,¹⁰⁻¹³ and polymeric materials.¹⁴⁻¹⁶

The development of LHSs has been accompanied by significant progress toward extending their applications. Recently, impressive work on the construction of LHSs for applications in aqueous environments has been reported. For instance, Wang *et al.* developed a supramolecular artificial LHS for photochemical catalysis,¹⁷ and Li *et al.* fabricated an efficient near-infrared-

emissive supramolecular LHS for imaging in the Golgi apparatus.¹⁸ Diao and co-workers reported stimulus-responsive light-harvesting complexes that show photocatalytic activity when exposed to light,¹⁹ and Klymchenko *et al.* reported light-harvesting probes that are based on polymer nanoparticles²⁰⁻²³ and that can be used for fluorescence resonance energy transfer (FRET)-based detection of oligonucleotides and nucleic acids.^{24,25} In addition, we have utilized artificial LHSs for highly efficient secondary energy transfer.²⁶ More recently, Tang *et al.* developed a conjugated polymeric supramolecular network that is based on aggregation-induced emission luminogens (AIEgens) and displays an ultrahigh antenna effect.¹⁴ AIEgens are thought to play an important role in LHSs, markedly enhancing fluorescence intensity by adopting tightly stacked, orderly spatial arrangements that prevent intramolecular fluorescence self-quenching.²⁷⁻²⁹ These previously reported results suggest that it would be significant to fabricate AIEgen-based LHS platforms for making full use of light energy.

Researchers have reported a number of artificial LHSs based on macrocycles such as cyclodextrins,^{30,31} pillar[*n*]arenes,³²⁻³⁵ calix[*n*]arenes,³⁶ and cucurbiturils.^{37,38} For example, amphiphilic sulfonatocalix[*n*]arenes ($n = 4-8$) are used widely in biomedical and biological applications because of their good water solubility and biocompatibility.³⁹ Sulfonatocalix[*n*]arenes contain a hydrophilic macrocyclic skeleton bearing hydrophobic alkyl chains and negatively charged sulfonate groups.⁴⁰ The alkyl chains participate in strong hydrophobic interactions in amphiphilic assemblies,⁴¹ and the sulfonate groups provide anchoring points that interact electrostatically with positively charged guest molecules.⁴² The ability of sulfonatocalix[*n*]arenes to engage in

College of Chemistry, State Key Laboratory of Elemento-Organic Chemistry, Nankai University, Tianjin 300071, P. R. China. E-mail: yuliu@nankai.edu.cn

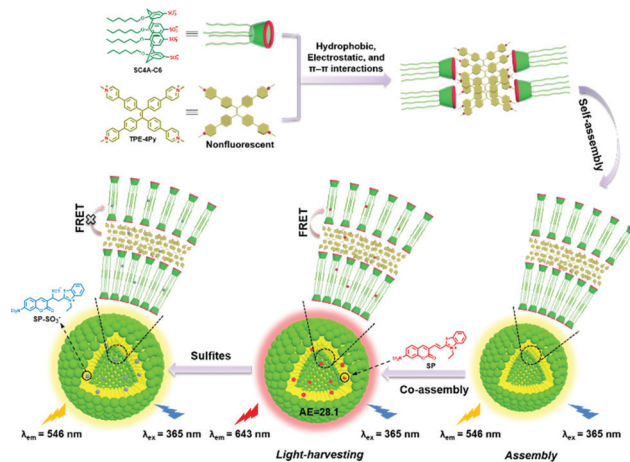
† Dedicated to the 100th anniversary of Chemistry at Nankai University.

‡ Electronic supplementary information (ESI) available: Experimental procedure, including synthesis and spectroscopic data of compounds. See DOI: 10.1039/d0tc05243d

both hydrophobic and electrostatic interactions suggests that they would be useful for constructing AIE-based LHSs that not only exhibit assembling-induced emission behavior⁴³ but also contain hydrophobic moieties that would facilitate co-assembly with functional fluorescent molecules to achieve a high antenna effect and efficient energy transfer.

An inherent limitation of fluorescence-based assays is the limited brightness of the currently available fluorescent dyes, some of which exhibit aggregation-caused quenching (ACQ).^{44,45} Therefore, a promising strategy for amplifying the brightness of such dyes is to use LHSs as energy donors. Strongly coupled energy donors can communicate *via* excitation energy migration, and then the energy can be transferred to an acceptor by means of FRET.⁴⁶ Meanwhile, spectral matching and adjustment of the distance between the donor and the acceptor minimizes energy loss, and surrounding the acceptor by multiple antenna chromophores favors high energy-transfer efficiency.⁴⁷ The combination of high energy-transfer efficiency and an antenna effect could amplify the signal generated by trace amounts of a dye, which would prevent dye self-quenching and reducing excitation powers of instrument equipment. Such an AIE-based supramolecular LHS might be useful for sensing small molecules such as sulfites, which are generated by inhalation of toxic SO₂ in addition to being produced endogenously from sulfur-containing amino acids.^{48–50} To our knowledge, sulfites have been widely used as common food additives and preservatives, enzyme inhibitors, and pharmaceutical products,^{51,52} meanwhile, studies have shown that excessive intake of sulfites can have harmful effects on cells and tissues, causing various health problems, including lung cancer, hives, and respiratory and cardiovascular disease.^{53–56} Moreover, endogenously produced SO₂ could regulate vascular smooth muscle tone and lower blood pressure due to the main existence forms of HSO₃[−] or SO₃^{2−}.^{57–59} Therefore, it is important to monitor the sulfites in living systems.⁶⁰ Considering the above reasons, we were interested in developing a supramolecular LHS that could be combined with a fluorescent probe to detect sulfites with signal amplification. Because sulfite is not overexpressed as a tumor marker, the cancer cells were selected as the cell model due to their easy cultivation.

Herein, we report a high-efficiency aqueous supramolecular LHS for sensing sulfites. The system comprises a tetraphenylethylene derivative (**TPE-4Py**) and an amphiphilic sulfonatocalix[4]arene (**SC4A-C6**), which are co-assembled with a sulfite probe (**SP**) (Scheme 1). In phosphate-buffered saline (PBS), aggregates composed of **TPE-4Py** and **SC4A-C6** displayed excellent AIE owing to the restricted rotation of the two molecules in the aggregates. After the **SP** (the acceptor) was loaded into the hydrophobic layer of the **TPE-4Py/SC4A-C6** assembly (the donor), the resulting assemblies showed an antenna effect of up to 28.1 and an energy-transfer efficiency of 75.2%, and an obvious signal amplification effect was observed. Importantly, these assemblies could be used to sense sulfites in A549 cells, with excellent ratiometric fluorescence signal output and response capability. Our supramolecular strategy for designing AIEgen-based assemblies provides an excellent platform for constructing supramolecular fluorescent cell sensors.



Scheme 1 Schematic illustration of the assembly of the LHS for sensing sulfites.

Results and discussion

First, we used fluorescence spectroscopy to investigate the effect of the solvent composition (H₂O/THF) on **TPE-4Py** aggregation (Fig. S1, ESI†). Increasing the water content from 10% to 99% had no obvious effect on the fluorescence spectrum of **TPE-4Py**, indicating that self-aggregation of **TPE-4Py** did not affect fluorescence intensity. However, addition of **SC4A-C6** to 99% aqueous **TPE-4Py** enhanced the fluorescence intensity at 550 nm by a factor of 30. This result demonstrates that **SC4A-C6** induced **TPE-4Py** self-assembly into a close-packed structure that restricted intramolecular rotation of **TPE-4Py**, which in turn resulted in an obvious AIE effect. A similar phenomenon was observed when the same experiment was carried out in PBS buffer, owing to calixarene-induced aggregation, which resulted in emission of a strong yellow fluorescence and slight change in the absorption spectrum (Fig. 1a and Fig. S2, ESI†).

Subsequently, we investigated the ability of **SC4A-C6** to induce **TPE-4Py** aggregation in more detail by measuring the optical transmittance at 600 nm at various **TPE-4Py** concentrations in PBS buffer solution. In the absence of **SC4A-C6**, no change in optical transmittance was observed as the **TPE-4Py** concentration was increased from 0.002 to 0.02 mM (Fig. S3a and b, ESI†), indicating that **TPE-4Py** could not aggregate in this concentration range. In contrast, when **SC4A-C6** was present, the optical transmittance decreased with increasing **TPE-4Py** concentration as supramolecular assemblies formed (Fig. S3c, ESI†). A plot of optical transmittance at 600 nm *versus* **TPE-4Py** concentration indicated that in the presence of **SC4A-C6**, the critical aggregation concentration was 10 μM (Fig. 1b); that is, the critical aggregation concentration of **TPE-4Py** was markedly decreased by complexation with **SC4A-C6**.

Next we determined the optimum **TPE-4Py/SC4A-C6** molar ratio (Fig. 1c and Fig. S4, ESI†). As the **SC4A-C6** concentration was increased, the transmittance at 600 nm initially decreased to a minimum of 97% and then increased to the original level. The minimum transmittance occurred at a **TPE-4Py/SC4A-C6**

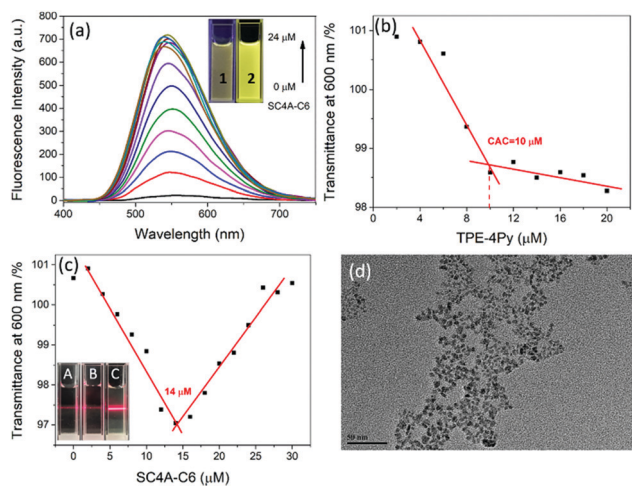


Fig. 1 (a) Fluorescence spectra of **TPE-4Py** (10 μM) at **SC4A-C6** concentrations of 0–24 μM in PBS buffer (10 mM, pH 7.4) ($\lambda_{\text{ex}} = 365$ nm; slits: 2.5/5 nm). Inset: Photographs of (1) **TPE-4Py** and (2) **TPE-4Py/SC4A-C6** solutions. (b) Dependence of optical transmittance at 600 nm on **TPE-4Py** concentration at a **SC4A-C6** concentration of 10 μM . (c) Dependence of optical transmittance at 600 nm on **SC4A-C6** concentration at a **TPE-4Py** concentration of 12 μM . Inset: Demonstration of Tyndall effects exhibited by (A) **SC4A-C6**, (B) **TPE-4Py**, and (C) **TPE-4Py/SC4A-C6**. (d) Transmission electron microscopy image of **TPE-4Py/SC4A-C6** assemblies.

molar ratio of 1.17 : 1, indicating that this was the best mixing ratio for the formation of amphiphilic assemblies. In addition, a mixture of **SC4A-C6** and **TPE-4Py** at a ratio of 1.17 : 1 in PBS buffer exhibited a clear Tyndall effect (Fig. 1c inset), indicating the formation of abundant nanoparticles. In contrast, solutions of **TPE-4Py** and **SC4A-C6** alone showed very weak Tyndall effects, indicating that neither the guest nor the host alone could efficiently form nanoscale aggregates under the same conditions. Furthermore, the morphology and size of the **TPE-4Py/SC4A-C6** assemblies were examined by means of transmission electron microscopy (Fig. 1d), which showed that the assemblies were spherical nanoparticles that had diameters of about 10 nm. The average zeta potential of the **TPE-4Py/SC4A-C6** assemblies was -32.9 mV (Fig. S5, ESI \ddagger), suggesting that their surfaces were negatively charged, which could be expected to improve the stability of the nanoparticles in PBS buffer.

To elucidate the driving force for assembly of **TPE-4Py** and **SC4A-C6**, we carried out some control experiments with **SC4A**, which lacks the alkyl chains. We found that **SC4A** did not enhance the fluorescence of **TPE-4Py** (Fig. S6, ESI \ddagger), indicating that assembly was driven not only by electrostatic interactions but also by hydrophobic interactions; that is, the alkyl chains played a key role in this system. We also found that when sodium dodecyl benzene sulfonate was present in the system, there was no obvious AIE effect. Taken together, the aforementioned results allow us to conclude that supramolecular nanoparticles formed by the process schematically illustrated in Scheme 1. The hydrophobic alkyl chains of **SC4A-C6** are packed together, and the inner and outer surfaces of the assemblies consist of the hydrophilic sulfonate groups of **SC4A-C6**, which

are exposed to the aqueous solution. The **SC4A-C6** and **TPE-4Py** molecules are held together by electrostatic interactions between the negative sulfonate groups and the positive pyridinium groups. The resulting aggregates are stabilized simultaneously by several synergistic noncovalent interactions—hydrophobic, electrostatic, and π - π interactions—which allow the **TPE-4Py** molecules to form stable, high-order aggregates with a short aggregation distance.

From the above analyses and discussions, we found that **SC4A-C6** clearly induced AIE from **TPE-4Py**, markedly enhancing the fluorescence intensity of the system and increasing the fluorescence quantum yield from 1.99% to 56.50% (Fig. S7a and b, ESI \ddagger). These findings indicate that **TPE-4Py/SC4A-C6** assemblies could serve as an ideal donor for the construction of an artificial LHS in PBS buffer. In addition, we expected that the interior of the **TPE-4Py/SC4A-C6** assemblies could be loaded with a functional fluorescent material. Some coumarin-based probes have been shown to display ACQ in aqueous solution as their concentration increases, suggesting that if we loaded such a probe into our system, high fluorescence intensity could be achieved at a relatively low probe dose. On the basis of these considerations, we synthesized coumarin-based cyanine probe **SP** to act as an acceptor. As we expected, the absorption band of **SP** overlapped well with the fluorescence emission band of the **TPE-4Py/SC4A-C6** assemblies (Fig. S8, ESI \ddagger), which was favorable for FRET. When **SP** was added to the **TPE-4Py/SC4A-C6** assemblies (the donor), their fluorescence intensity at 546 nm decreased gradually with increasing **SP** concentration, while the fluorescence emission of **SP** (the acceptor) at 643 nm increased upon excitation at 365 nm (Fig. 2a). Meanwhile, the color of the fluorescence changed from the light yellow of the **TPE-4Py/SC4A-C6** assemblies to the bright orange-red of **TPE-4Py/SC4A-C6/SP**. The fluorescence quantum yield was 57.63% (Fig. S7c, ESI \ddagger), indicating efficient energy transfer from the donor to the acceptor. In control experiments, the fluorescence of **SP** alone at the same concentration was negligible upon excitation at 533 nm, with a fluorescence quantum yield close to zero (Fig. S7d, ESI \ddagger); and an **SC4A-C6/SP** complex also exhibited very weak fluorescence intensity under the same conditions (Fig. S9a, ESI \ddagger). In the absence of **SC4A-C6**, addition of **SP** to **TPE-4Py** resulted in no obvious fluorescence change (Fig. S9b, ESI \ddagger), demonstrating that there was no interaction between **TPE-4Py** and **SP** and that **SC4A-C6** played an important role in this LHS.

To explore the light-harvesting process further, we carried out some fluorescence decay experiments. Compared with the decay curve of **TPE-4Py** ($\tau = 0.05$ ns), the decay curve of the **TPE-4Py/SC4A-C6** assemblies showed higher fluorescence lifetimes ($\tau_1 = 2.79$ ns and $\tau_2 = 5.62$ ns; Fig. 2b). Furthermore, the corresponding fluorescence lifetimes of the **TPE-4Py/SC4A-C6/SP** assemblies were only 1.11 and 3.31 ns, respectively. In addition, the average fluorescence lifetime values of **TPE-4Py/SC4A-C6** and **TPE-4Py/SC4A-C6/SP** were estimated for 4.58 ns and 2.78 ns (Fig. S10, ESI \ddagger), respectively, confirming energy transfer from the **TPE-4Py/SC4A-C6** donor to the **SP** acceptor.

Next we investigated the energy-transfer efficiency and antenna effect of the **TPE-4Py/SC4A-C6/SP** assemblies because

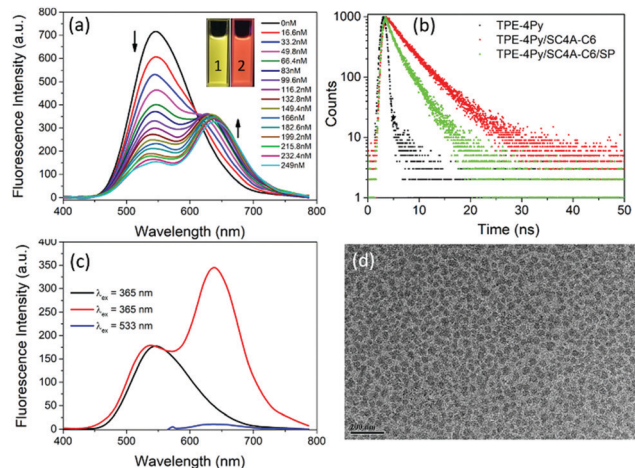


Fig. 2 (a) Fluorescence spectra of **TPE-4Py/SC4A-C6** (**[TPE-4Py]** = 12 μM , **[SC4A-C6]** = 14 μM) in PBS (10 mM, pH 7.4) at **SP** concentrations of 0–249 nM (λ_{ex} = 365 nm; slits: 2.5/5 nm). Inset: Photographs of (1) **TPE-4Py/SC4A-C6** and (2) **TPE-4Py/SC4A-C6/SP** solutions under UV light (365 nm) (**[TPE-4Py]** = 12 μM , **[SC4A-C6]** = 14 μM , **[SP]** = 216 nM). (b) Fluorescence decay profiles of **TPE-4Py**, **TPE-4Py/SC4A-C6**, and **TPE-4Py/SC4A-C6/SP** in PBS solution (**[TPE-4Py]** = 12 μM , **[SC4A-C6]** = 14 μM , **[SP]** = 216 nM) (λ_{ex} = 365 nm, λ_{em} = 350–800 nm). (c) Antenna effect maxima of **TPE-4Py/SC4A-C6/SP** in PBS buffer solution. Red line (assembly emission, λ_{ex} = 365 nm, **[TPE-4Py]** = 12 μM , **[SC4A-C6]** = 14 μM , **[SP]** = 216 nM), blue line (**SP** emission, λ_{ex} = 533 nm, **[SP]** = 216 nM). The black line represents the fluorescence spectrum of **TPE-4Py/SC4A-C6**, which was normalized according to the fluorescence intensity at 546 nm of the red line. (d) Transmission electron microscopy image of **TPE-4Py/SC4A-C6/SP** assemblies.

these values are important measures of the performance of artificial LHSs. On the basis of the fluorescence quenching rate of the **TPE-4Py/SC4A-C6** assemblies, the energy-transfer efficiency was calculated to be 75.2% at a donor/acceptor molar ratio of 56 : 1 (Fig. S11, ESI \ddagger), and the antenna effect was 28.1 at this ratio (Fig. 2c). Compared with the assembly of **TPE-4Py/SC4A** and **TPE-4Py/SC4A-C6**, we found that the hydrophobic alkyl chains of **SC4A-C6** play an important role in constructing LHSs. Hence, we considered that **SP** was inclined to the hydrophobic part of **TPE-4Py/SC4A-C6** because of its lipophilicity, so that the FRET effect could be realized efficiently. The possible binding mode was similar to previous reported LHS.^{17,18,31,32} The 56 : 1 ratio of **TPE-4Py/SC4A-C6/SP** was the optimal one that displayed the highest fluorescence intensity, and too much proportion of the **SP** will cause the fluorescence quenching of **TPE-4Py/SC4A-C6/SP** due to the ACQ effect of **SP**. In addition, comparison of **SP** alone with the **TPE-4Py/SC4A-C6** assemblies showed a clear ACQ phenomenon as the concentration of **SP** was increased, and displayed the highest fluorescence intensity at 16 μM (Fig. S12a and c, ESI \ddagger). While, in this LHS, nanomolar **SP** (216 nM) could exhibit superior fluorescence to **SP** alone under the same measuring parameter, demonstrating that our strategy effectively improved the fluorescence intensity of **SP** in trace concentrations. Moreover, the fluorescence spectra of **SC4A-C6/SP** at different concentrations in PBS buffer solution were tested and compared with the results of **SP** (Fig. S12b and c, ESI \ddagger). After **SC4A-C6** was added in the **SP** solution, the highest fluorescence intensity of **SC4A-C6/SP** was

changed at 4 μM , accompanied by slightly higher in fluorescence intensity than **SP** alone, demonstrating that the supramolecular assembly strategy was in favor of the utilization of the probe at a relatively low dose. The above-described results indicate that the **TPE-4Py/SC4A-C6** assemblies functioned as an excellent light-harvesting platform for improving the luminescence behavior of a fluorescent probe in an aqueous environment.

It is well known that **SP** can undergo Michael addition reactions with sulfites, therefore we evaluated the response of **TPE-4Py/SC4A-C6/SP** to sulfites.⁴⁸ Upon addition of HSO_3^- , an excellent ratiometric fluorescence response was observed. As the HSO_3^- concentration was increased, the intensity of the emission at 643 nm gradually decreased and that of the emission at 546 nm increased; the separation between the maxima was large (approximately 97 nm, Fig. 3a and b). The dramatic fluorescence enhancement at 546 nm was attributed to a Michael addition reaction between HSO_3^- and **SP**, which disrupted the π - π conjugation in **SP** and then blocked light harvesting from the assembly by **SP**, which subsequently restored the fluorescence of **TPE-4Py/SC4A-C6**. The fluorescence changes induced by the addition of HSO_3^- to **TPE-4Py/SC4A-C6/SP** were observable by the naked eye (Fig. 3a, inset). The $I_{546\text{nm}}/I_{643\text{nm}}$ ratio for **TPE-4Py/SC4A-C6/SP** was linearly related to the HSO_3^- concentration; an 8-fold enhancement in the ratio was observed, and the limit of detection for HSO_3^- was determined to be 21 nM on the basis of a S/N ratio of 3 (Fig. S13, ESI \ddagger). The time-course of the fluorescence response spectrum indicated that the sensing process was complete within 8 min (Fig. 3c). Subsequently, the NMR tests were implemented to identify the mechanism between the sulfite and **SP** loading in LHS. The NMR spectra of

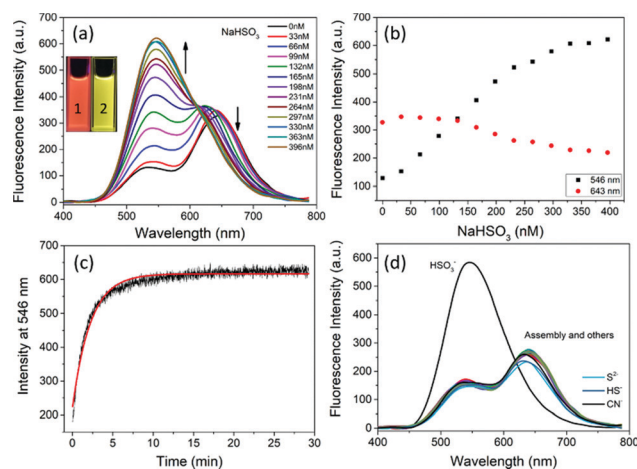


Fig. 3 (a) Fluorescence spectra of **TPE-4Py/SC4A-C6/SP** (**[TPE-4Py]** = 12 μM , **[SC4A-C6]** = 14 μM , **[SP]** = 216 nM) upon gradual addition of HSO_3^- in PBS buffer (pH 7.4, 10 mM). Each spectrum was recorded 8 min after the addition of HSO_3^- . (b) Effect of HSO_3^- concentration on the fluorescence intensities of **TPE-4Py/SC4A-C6/SP** at 546 and 643 nm. (c) Time-course of the fluorescence response spectrum of **TPE-4Py/SC4A-C6/SP** toward HSO_3^- (0.4 mM) in PBS buffer. (d) Fluorescence spectra of **TPE-4Py/SC4A-C6/SP** in the presence of HSO_3^- , F^- , Cl^- , Br^- , I^- , PO_4^{3-} , HPO_4^{2-} , H_2PO_4^- , NO_3^- , NO_2^- , SCN^- , $\text{S}_2\text{O}_3^{2-}$, SO_4^{2-} , CO_3^{2-} , AcO^- , ClO^- , Cys, GSH, S^{2-} , HS^- , and CN^- .

SP, SP + HSO₃⁻, TPE-4Py/SC4A-C6/SP and TPE-4Py/SC4A-C6/SP + HSO₃⁻ were measured, respectively. As shown in Fig. S14 (ESI[†]), the HSO₃⁻ could attack to hemicyanine moieties of SP *via* the nucleophilic addition reaction, which was consistent with previous reported research.⁴⁸ When SP is loaded into nanoparticles, the same reaction mechanism between HSO₃⁻ and SP was found, while, the chemical shift changes slightly, because it was encapsulated in the nanoparticles. Therefore, the above results demonstrated that the reaction mechanism between sulfite and SP in LHS was the nucleophilic addition reaction.

Next, the detection results of SC4A-C6/SP and SP toward the HSO₃⁻ ion were tested and compared with the detection results of a host-guest system toward the HSO₃⁻ ion under the same conditions. As shown in Fig. S15a and c (ESI[†]), SP displayed the best detectability for HSO₃⁻. After being assembled with SC4A-C6 *via* host-guest interaction, the fluorescence intensity was quenched because of the photoinduced electron transfer (PET) effect of SC4A-C6, and the detection capability of the SC4A-C6/SP was also passivated (Fig. S15b and d, ESI[†]). The fluorescence intensity of SC4A-C6/SP toward HSO₃⁻ increased, and then it decreased. The reason may derive from the interference of HSO₃⁻ to host-guest interaction between SC4A-C6 and SP, which make the SP escaped from the cavity of SC4A-C6 with the destruction of the PET process, then the additional addition of HSO₃⁻ could react with SP, showing the decrease of fluorescence intensity. Comparing the detection results among SP, SC4A-C6/SP and TPE-4Py/SC4A-C6/SP toward HSO₃⁻, we found that the SP showed the best detectability for HSO₃⁻ than others, but the fluorescence intensity is much weaker than TPE-4Py/SC4A-C6/SP. TPE-4Py/SC4A-C6/SP displayed better detectability than SC4A-C6/SP, and higher fluorescence intensity than SP, demonstrating that TPE-4Py/SC4A-C6/SP could amplify the signal of the SP, accompanied by appropriate detectability for HSO₃⁻.

In addition, we evaluated the selectivity of TPE-4Py/SC4A-C6/SP for sulfites by testing other anions (Fig. 3d), none of which induce any observable fluorescent changes. Even the biothiols cysteine (Cys) and glutathione (GSH), which are present in large quantities in cells, displayed no obvious interaction with the nanoparticles. Indeed, some nucleophiles, such as cyanide and sulfide ions, can also attack hemicyanine moieties of SP *via* the nucleophilic addition reaction. However, after addition of CN⁻, S²⁻ and HS⁻ to the solution of TPE-4Py/SC4A-C6/SP, no obvious change in fluorescence intensity was found. The reason may result from the inhibition of reaction between SP and CN⁻, S²⁻ and HS⁻ in LHS, just like the relatively lower detectability between SP and HSO₃⁻ in LHS than not being in LHS. The results demonstrated that the bonding ability between HSO₃⁻ and TPE-4Py/SC4A-C6/SP was stronger than others. Compared with TPE-4Py/SC4A-C6/SP, SP showed very weak fluorescence at the same concentration (Fig. 2c), which limits its signal output. Hence, our results demonstrate that TPE-4Py/SC4A-C6/SP can serve as a specific ratiometric fluorescent probe for the detection of HSO₃⁻. Next, we evaluated the influence of temperatures and pH values on the FRET behavior for the assembly of TPE-

4Py/SC4A-C6/SP and the HSO₃⁻ ion sensing. As shown in Fig. S16a and b (ESI[†]), the FRET behavior for the assembly of TPE-4Py/SC4A-C6/SP was not disturbed by different pH values, and the assembly displayed the best response for HSO₃⁻ in the pH range (6–10). In addition, the temperature dependent FRET processes of TPE-4Py/SC4A-C6/SP and the HSO₃⁻ ion recognition process were also measured (Fig. S16c and d, ESI[†]). Upon heating, the fluorescence intensities of both the processes displayed continuous slight drop in the range of 25–55 °C because of the thermal quenching effect.⁵¹ Therefore, the assembly of TPE-4Py/SC4A-C6/SP could be used to detect HSO₃⁻ in the pH range (6–10) in cells, and the temperatures had little effect on the detection.

To demonstrate the utility of the TPE-4Py/SC4A-C6/SP assemblies for detecting the sulfites in living cells, we carried out experiments with A549 cells. Before that, the cytotoxicity of assemblies was determined by CCK-8 assays. It was found that TPE-4Py/SC4A-C6/SP assemblies have a very minor effect on cell viability (Fig. S17, ESI[†]). Subsequently, as shown in Fig. 4a–d, cells treated with TPE-4Py displayed very weak yellow and red fluorescence, whereas strong yellow fluorescence and weak red fluorescence were observed when the cells were incubated with TPE-4Py/SC4A-C6 for 3 h (Fig. 4e–h). These findings demonstrate that the TPE-4Py/SC4A-C6 assemblies could permeate the cells and give a clear fluorescence signal. Furthermore, when the cells were treated with TPE-4Py/SC4A-C6/SP, we observed bright red fluorescence accompanied by a decrease in the yellow fluorescence, demonstrating FRET between TPE-4Py/

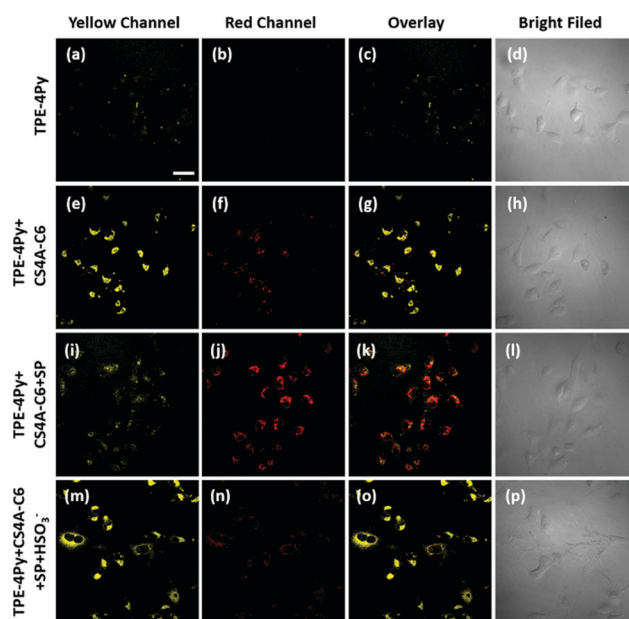


Fig. 4 Confocal fluorescence images of living A549 cells incubated with (a–d) TPE-4Py, (e–h) TPE-4Py/SC4A-C6, and (i–l) TPE-4Py/SC4A-C6/SP for 3 h and (m–p) images of TPE-4Py/SC4A-C6/SP-loaded A549 cells incubated with 0.4 mM HSO₃⁻ for an additional 0.5 h (scale bar = 40 μm). The excitation wavelengths for the yellow and red channels were 405 nm, and the emission wavelength ranges for the yellow and red channels were 460–560 and 610–710 nm, respectively.

SC4A-C6 and SP (Fig. 4i-l). After the assembly-loaded cells were stimulated with NaHSO₃ (0.4 mM), the red fluorescence vanished, and the disappearance was accompanied by the recovery of strong fluorescence in the yellow channel (Fig. 4m-p). These findings confirm that the light-harvesting TPE-4Py/SC4A-C6/SP assemblies could be used to sense HSO₃⁻ in living cells.

Conclusions

In summary, we have fabricated a highly efficient supramolecular LHS for the detection of sulfites in aqueous environments, including living cells. In this three-component system, SC4A-C6 induced TPE-4Py to aggregate in PBS buffer solution, and the aggregation was accompanied by enhanced fluorescence intensity. The resulting TPE-4Py/SC4A-C6 assemblies acted as a FRET donor to a fluorescent probe (SP), showing clear signal amplification with an antenna effect of up to 28.1 and an energy-transfer efficiency of 75.2%. The TPE-4Py/SC4A-C6/SP assemblies could be used to detect sulfites in living cells, displaying excellent ratiometric fluorescence signal output and response capability. This supramolecular strategy for making use of AIEgens by introducing them into a LHS to improve the performance of an ACQ probe can be expected to facilitate the development of useful fluorescent materials.

Experimental

All chemical reagents and solvents for synthesis were purchased from commercial sources (Aladdin Industrial Corporation, Tokyo Chemical Industry and Sigma-Aldrich Chemical) and were used without further purification. Ultrapure water was used after passing through a water ultra-purification system. ¹H NMR and ¹³C NMR spectra were recorded on an Ascend 400 MHz (BRUKER) at room temperature. High-resolution mass spectra (HRMS) were measured on 6520 Q-TOF LC/MS (Agilent). Absorption spectra were recorded on a UV-vis spectrophotometer (UV-2700, Shimadzu), and steady-state fluorescence emission spectra were recorded in a conventional quartz cell (10 × 10 × 45 mm) at 25 °C on a Varian Cary Eclipse equipped with a Varian Cary single-cell Peltier accessory to control temperature. Absolute fluorescence quantum yields were recorded on a FLS980 instrument (Edinburg Instruments Ltd, Livingstone, UK). Confocal fluorescence and bright-field imaging were recorded with FV1000 (Olympus).

Solution preparation

TPE-4Py and SP stock solution was made by dissolving them in DMSO. SC4A, SC4A-C6 and sodium dodecyl benzene sulfonate were dissolved in water. All the above stock solution was prepared to a final concentration of 1 mM and kept at -20 °C before use. GSH, Cys, H₂O₂ and other analyses were dissolved in water. Mixing was usually done by adding analyte solution (for example, GSH solution) into probe solution.

Calculation of the distance between TPE-4Py and SP in LHS

In FRET, Förster showed that the efficiency of this process (E) depends on the inverse sixth-distance between the donor and acceptor (1).⁶¹ R_0 is the distance at which half of the energy is transferred.⁶² In addition, E can also be calculated by experimental measurement (2). I_{DA}/I_D represented the fluorescence intensity of the donor with and without the receptor, respectively. Hence, the distances between TPE-4Py and SP in LHS were estimated to be 47 Å, measured under the conditions of [TPE-4Py] = 12 μM, [SC4A-C6] = 14 μM, [SP] = 216 nM, and λ_{ex} = 365 nm.

$$E = 1/[1 + (R/R_0)^6] \quad (1)$$

$$E = 1 - I_{DA}/I_D \quad (2)$$

Calculation of energy-transfer efficiency (Φ_{ET})

Energy-transfer efficiency (Φ_{ET}), the fraction of the absorbed energy that is transferred to the acceptor, is experimentally measured as a ratio of the fluorescence intensities of the donor in the absence and presence of the acceptor (I_D and I_{DA}).³⁶

The energy-transfer efficiency (Φ_{ET}) was calculated as 75.2% in PBS buffer, measured under the conditions of [TPE-4Py] = 12 μM, [SC4A-C6] = 14 μM, [SP] = 216 nM, and λ_{ex} = 365 nm.

$$\Phi_{ET} = 1 - \frac{I_{DA}}{I_D}$$

Calculation of the antenna effect (AE)

The antenna effect at certain concentrations of the donor and acceptor equals the ratio of the emission intensity at 643 nm of the acceptor upon excitation of the donor.³⁶

$$\text{Antenna effect} = \frac{I_{A+D}^{643 \text{ nm}}(\lambda_{ex}=365 \text{ nm}) - I_{D}^{643 \text{ nm}}(\lambda_{ex}=365 \text{ nm})}{I_{A+D}^{643 \text{ nm}}(\lambda_{ex}=533 \text{ nm})}$$

$I_{A+D}(\lambda_{ex} = 365 \text{ nm})$ and $I_{A+D}(\lambda_{ex} = 533 \text{ nm})$ are the fluorescence intensities of excitation of the donor at 365 nm and direct excitation of the acceptor at 533 nm, respectively. $I_D(\lambda_{ex} = 365 \text{ nm})$ is the fluorescence intensities of the acceptor at 365 nm. The antenna effect value was calculated to be 28.1 in PBS buffer, measured under the conditions of [TPE-4Py] = 12 μM, [SC4A-C6] = 14 μM, [SP] = 216 nM, and λ_{ex} = 365 nm.

Cell culture and fluorescence imaging experiment

A549 cells were grown in F12 medium containing 10% FBS, 1% penicillin, and 1% streptomycin at 37 °C in 5% CO₂. The cells were plated on confocal dish and allowed to adhere for 24 hours. For a confocal fluorescence imaging experiment, the cells were washed with PBS and then incubated with targets in culture medium for another 3 h at 37 °C. The cell staining experiment was investigated after washing with PBS 3 times.

Conflicts of interest

There are no conflicts to declare.

Acknowledgements

This work was supported by the National Natural Science Foundation of China (grant no. 21807038, 21772099 and 21861132001), the China Postdoctoral Science Foundation (2019M651006), and the Science and Technology Research Project of the Department of Education of Jilin Province (No. JJKH20191008KJ).

Notes and references

- U. Hahn, M. Gorka, F. Vögtle, V. Vicinelli, P. Ceroni, M. Maestri and V. Balzani, *Angew. Chem., Int. Ed.*, 2002, **41**, 3595–3598.
- L. Jullien, J. Canceill, B. Valeur, E. Bardez, J.-P. Lefèvre, J.-M. Lehn, V. Marchi-Artzner and R. Pansu, *J. Am. Chem. Soc.*, 1996, **118**, 5432–5442.
- P. Z. Chen, Y. X. Weng, L. Y. Niu, Y. Z. Chen, L. Z. Wu, C. H. Tung and Q. Z. Yang, *Angew. Chem., Int. Ed.*, 2016, **55**, 2759–2763.
- X. Zhang, Z. K. Chen and K. P. Loh, *J. Am. Chem. Soc.*, 2009, **131**, 7210–7211.
- K. Acharyya, S. Bhattacharyya, H. Sephehpour, S. Chakraborty, S. Lu, B. Shi, X. Li, P. S. Mukherjee and P. J. Stang, *J. Am. Chem. Soc.*, 2019, **141**, 14565–14569.
- H. Q. Peng, Y. Z. Chen, Y. Zhao, Q. Z. Yang, L. Z. Wu, C. H. Tung, L. P. Zhang and Q. X. Tong, *Angew. Chem., Int. Ed.*, 2012, **51**, 2088–2092.
- G. Chadha, Q. Z. Yang and Y. Zhao, *Chem. Commun.*, 2015, **51**, 12939–12942.
- Q. Zou, K. Liu, M. Abbas and X. Yan, *Adv. Mater.*, 2016, **28**, 1031–1043.
- H. Kashida, H. Azuma, R. Maruyama, Y. Araki, T. Wada and H. Asanuma, *Angew. Chem., Int. Ed.*, 2020, **59**, 11360–11363.
- S. Inagaki, O. Ohtani, Y. Goto, K. Okamoto, M. Ikai, K. Yamanaka, T. Tani and T. Okada, *Angew. Chem., Int. Ed.*, 2009, **48**, 4042–4046.
- K. V. Rao, K. K. Datta, M. Eswaramoorthy and S. J. George, *Angew. Chem., Int. Ed.*, 2011, **50**, 1179–1184.
- H. Takeda, Y. Goto, Y. Maegawa, T. Ohsuna, T. Tani, K. Matsumoto, T. Shimada and S. Inagaki, *Chem. Commun.*, 2009, 6032–6034, DOI: 10.1039/b910528j.
- I. Nabiev, A. Rakovich, A. Sukhanova, E. Lukashev, V. Zagidullin, V. Pachenko, Y. P. Rakovich, J. F. Donegan, A. B. Rubin and A. O. Govorov, *Angew. Chem., Int. Ed.*, 2010, **49**, 7217–7221.
- L. Xu, Z. Wang, R. Wang, L. Wang, X. He, H. Jiang, H. Tang, D. Cao and B. Z. Tang, *Angew. Chem., Int. Ed.*, 2020, **59**, 9908–9913.
- X. Zhu, J.-X. Wang, L.-Y. Niu and Q.-Z. Yang, *Chem. Mater.*, 2019, **31**, 3573–3581.
- F. Pu, L. Wu, E. Ju, X. Ran, J. Ren and X. Qu, *Adv. Funct. Mater.*, 2014, **24**, 4549–4555.
- M. Hao, G. Sun, M. Zuo, Z. Xu, Y. Chen, X. Y. Hu and L. Wang, *Angew. Chem., Int. Ed.*, 2020, **59**, 10095–10100.
- X. M. Chen, Q. Cao, H. K. Bisoyi, M. Wang, H. Yang and Q. Li, *Angew. Chem., Int. Ed.*, 2020, **59**, 10493–10497.
- Y. Sun, F. Guo, T. Zuo, J. Hua and G. Diao, *Nat. Commun.*, 2016, **7**, 12042.
- A. Reisch and A. S. Klymchenko, *Small*, 2016, **12**, 1968–1992.
- K. Trofymchuk, A. Reisch, P. Didier, F. Frasn, P. Gilliot, Y. Mely and A. S. Klymchenko, *Nat. Photon.*, 2017, **11**, 657–663.
- A. Reisch, P. Didier, L. Richert, S. Oncul, Y. Arntz, Y. Mely and A. S. Klymchenko, *Nat. Commun.*, 2014, **5**, 4089.
- B. Andreiuk, A. Reisch, E. Bernhardt and A. S. Klymchenko, *Chem. – Asian J.*, 2019, **14**, 836–846.
- N. Melnychuk, S. Egloff, A. Runser, A. Reisch and A. S. Klymchenko, *Angew. Chem., Int. Ed.*, 2020, **59**, 6811–6818.
- C. Severi, N. Melnychuk and A. S. Klymchenko, *Biosens. Bioelectron.*, 2020, **168**, 112515.
- J. J. Li, H. Y. Zhang, X. Y. Dai, Z. X. Liu and Y. Liu, *Chem. Commun.*, 2020, **56**, 5949–5952.
- W. Xu, D. Wang and B. Z. Tang, *Angew. Chem., Int. Ed.*, 2020, DOI: 10.1002/anie.202005899.
- Y. Wang, J. Nie, W. Fang, L. Yang, Q. Hu, Z. Wang, J. Z. Sun and B. Z. Tang, *Chem. Rev.*, 2020, **120**, 4534–4577.
- Y. Li, Y. Dong, L. Cheng, C. Qin, H. Nian, H. Zhang, Y. Yu and L. Cao, *J. Am. Chem. Soc.*, 2019, **141**, 8412–8415.
- D. Zhang, Y. Liu, Y. Fan, C. Yu, Y. Zheng, H. Jin, L. Fu, Y. Zhou and D. Yan, *Adv. Funct. Mater.*, 2016, **26**, 7652–7661.
- J. J. Li, Y. Chen, J. Yu, N. Cheng and Y. Liu, *Adv. Mater.*, 2017, **29**, e1701905.
- S. Guo, Y. Song, Y. He, X. Y. Hu and L. Wang, *Angew. Chem., Int. Ed.*, 2018, **57**, 3163–3167.
- C. L. Sun, H. Q. Peng, L. Y. Niu, Y. Z. Chen, L. Z. Wu, C. H. Tung and Q. Z. Yang, *Chem. Commun.*, 2018, **54**, 1117–1120.
- Y. Zhu, L. Xu, L. Wang, H. Tang and D. Cao, *Chem. Commun.*, 2019, **55**, 5910–5913.
- L. B. Meng, D. Li, S. Xiong, X. Y. Hu, L. Wang and G. Li, *Chem. Commun.*, 2015, **51**, 4643–4646.
- Z. Xu, S. Peng, Y. Y. Wang, J. K. Zhang, A. I. Lazar and D. S. Guo, *Adv. Mater.*, 2016, **28**, 7666–7671.
- F. Qiao, Z. Yuan, Z. Lian, C.-Y. Yan, S. Zhuo, Z.-Y. Zhou and L.-B. Xing, *Dyes Pigm.*, 2017, **146**, 392–397.
- H.-J. Kim, P. C. Nandajan, J. Gierschner and S. Y. Park, *Adv. Funct. Mater.*, 2018, **28**, 1705141.
- W. C. Geng, J. L. Sessler and D. S. Guo, *Chem. Soc. Rev.*, 2020, **49**, 2303–2315.
- P. Li, Y. Chen and Y. Liu, *Chin. Chem. Lett.*, 2019, **30**, 1190–1197.
- H. B. Cheng, Y. M. Zhang, Y. Liu and J. Y. Yoon, *Chem*, 2019, **5**, 553–574.
- H. T. Feng, Y. Li, X. Duan, X. Wang, C. Qi, J. W. Y. Lam, D. Ding and B. Z. Tang, *J. Am. Chem. Soc.*, 2020, **142**, 15966–15974.
- X. Ma, J. Wang and H. Tian, *Acc. Chem. Res.*, 2019, **52**, 738–748.

- 44 C. Zhang, H. Xie, T. Zhan, J. Zhang, B. Chen, Z. Qian, G. Zhang, W. Zhang and J. Zhou, *Chem. Commun.*, 2019, **55**, 9444–9447.
- 45 B. Chen, C. Li, J. Zhang, J. Kan, T. Jiang, J. Zhou and H. Ma, *Chem. Commun.*, 2019, **55**, 7410–7413.
- 46 Y. Jiang and J. McNeill, *Chem. Rev.*, 2017, **117**, 838–859.
- 47 T. Xiao, W. Zhong, L. Zhou, L. Xu, X.-Q. Sun, R. B. P. Elmes, X.-Y. Hu and L. Wang, *Chin. Chem. Lett.*, 2019, **30**, 31–36.
- 48 Y. Q. Sun, J. Liu, J. Zhang, T. Yang and W. Guo, *Chem. Commun.*, 2013, **49**, 2637–2639.
- 49 Z. Liu, S. Guo, J. Piao, X. Zhou and X. Wu, *RSC Adv.*, 2014, **4**, 54554–54557.
- 50 W. Zhang, F. Huo, Y. Yue, Y. Zhang, J. Chao, F. Cheng and C. Yin, *J. Am. Chem. Soc.*, 2020, **142**, 3262–3268.
- 51 T. T. K. Cuc, P. Q. Nhien, T. M. Khang, C.-C. Weng, C.-H. Wu, B.-T. B. Hue, Y.-K. Li, J. I. Wu and H.-C. Lin, *Chem. Mater.*, 2020, **32**, 9371–9389.
- 52 Y. Yao, Q. Sun, Z. Chen, R. Huang, W. Zhang and J. Qian, *Talanta*, 2018, **189**, 429–436.
- 53 Y. Zhang, L. Guan, H. Yu, Y. Yan, L. Du, Y. Liu, M. Sun, D. Huang and S. Wang, *Anal. Chem.*, 2016, **88**, 4426–4431.
- 54 X. Zhou, S. Lee, Z. Xu and J. Yoon, *Chem. Rev.*, 2015, **115**, 7944–8000.
- 55 V. S. Lin, W. Chen, M. Xian and C. J. Chang, *Chem. Soc. Rev.*, 2015, **44**, 4596–4618.
- 56 H. Zhang, S. Xue and G. Feng, *Sens. Actuators, B*, 2016, **231**, 752–758.
- 57 J. Xu, D. J. Zheng, M. M. Su, Y. C. Chen, Q. C. Jiao, Y. S. Yang and H. L. Zhu, *Org. Biomol. Chem.*, 2018, **16**, 8318–8324.
- 58 X. Xie, C. Yin, Y. Yue, J. Chao and F. Huo, *Sens. Actuators, B*, 2018, **277**, 647–653.
- 59 K.-N. Wang, Y. Zhu, M. Xing, D. Cao, R. Guan, S. Zhao, Z. Liu and Z.-W. Mao, *Sens. Actuators, B*, 2019, **295**, 215–222.
- 60 X. Kong, M. Li, B. Dong, N. Zhang, W. Song, Y. Lu and W. Lin, *Analyst*, 2019, **144**, 4371–4379.
- 61 P. R. Selvin, *Nat. Struct. Biol.*, 2000, **7**, 730–734.
- 62 K. E. Sapsford, L. Berti and I. L. Medintz, *Angew. Chem., Int. Ed.*, 2006, **45**, 4562–4589.